HCl Vapor-Induced Structural Rearrangements of *n*-Alkanoate Self-Assembled Monolayers on Ambient Silver, Copper, and Aluminum Surfaces

Yu-Tai Tao,* Geoffrey D. Hietpas,† and David L. Allara*,†,‡

Contribution from the Institute of Chemistry, Academia Sinica, Taipei, Taiwan, Republic of China, and Departments of Chemistry and Materials Science and Engineering, Materials Research Institute, Pennsylvania State University, University Park, Pennsylvania 16802

Received March 1, 1996[⊗]

Abstract: Exposure to HCl vapor of highly organized self-assembled monolayers (SAMs) of *n*-alkanoic acids on native oxide-covered Ag, Cu, and Al surfaces results in a variety of structural changes strongly dependent on the specific SAM. Using infrared spectroscopy (IRS) and wetting measurements, it was observed that while SAMs on Al surfaces show no effects of HCl exposure over periods of minutes, exposure of SAMs on Ag and Cu over just periods of seconds induces protonation of the carboxylate head groups and severe reorganization of the film into different structural forms of the initial *n*-alkanoic acid. For the Ag SAMs of *n*-tridecanoic acid (C13) and shorter chains, disordered states of the acid are produced which upon ambient storage revert back to a carboxylate state with much less order than the initial SAM. However, for C14 and longer chains, protonation occurs to give crystalline forms of the acid. For the C16 SAM, the original structure of all-*trans* chains, tilted at 19−20° from the surface normal, converts to discreet monoclinic crystallites, estimated from the IRS data to be ∼5 nm in thickness and oriented with the {010} and/or {001} surface planes parallel to the substrate surface. After 7 days ambient storage reversion to the original SAM structure occurs, but for longer chains (e.g., C24) reversal is incomplete. While generally similar results are observed for SAMs on copper, the specific deprotonation and reorganization rates are faster than on Ag and only partial reversibility is observed. These different behaviors are interpreted in terms of a combination of differences in intermolecular interactions, headgroup−substrate interactions, and reactivities of the metal surfaces toward HCl and ambient O_2.

1. Introduction

Self-assembled monolayers (SAMs) on solid substrates are becoming of increasing interest as candidates for a variety of applications.[1] One of the prime requirements for most applications is monolayer stability. For example, in the case of protective substrate coatings, it is critical that the monolayers maintain a high degree of integrity in order to provide a continuous barrier against permeation of corrosive or etching agents.[2−5] A major issue for these applications is the time-dependent stability of the molecular packing under conditions of chemical stress, but little information appears to be available with respect to both the mechanisms and dynamics of the molecular level processes, e.g., adsorbate diffusion and structural rearrangement, which will ensue upon chemical attack. One class of SAMs where this issue is important is *n*-alkanoic acids, chemisorbed as carboxylates, on the basic native oxides of corrosable metals such as Al, Ag, and Cu.[6−8] These SAMs can be formed readily by simple solution and/or gas-phase exposure of freshly prepared substrates to the alkanoic acids and the resultant films can be densely packed with extremely high resistance to wetting by water and long-chain hydrocarbons, thus constituting a potentially useful protective coating for the substrate metals. This latter aspect seems particularly relevant since it has been observed that for the case of Ag, SAMs of the long-chain acids, e.g., *n*-$C_{15}H_{31}CO_2H$, are crystalline[7] and thus provide extremely dense overlayers for the metal substrate. For reference, a schematic of the general structure of these SAMs is shown in Figure 1.

With the objective of studying the time-dependent structural characteristics of SAMs after chemical attack, we selected the above cases of highly organized *n*-alkanoic acids on the ambient surfaces of Cu, Ag, and Al. The molecular structures of the initial SAMs were first rigorously characterized by quantitative infrared vibrational spectroscopy (IRS), generally confirming the previously derived structures, but in some cases providing significant details beyond those previously reported. Following an earlier preliminary study,[9] these SAMs then were subjected to severe chemical stress by exposure to HCl vapor with the expectation of inducing both protonation of the carboxylate groups and strong chemical changes in the metal oxide/metal

* Academia Sinica.
† Department of Chemistry, Pennsylvania State University.
‡ Department of Materials Science and Engineering, Pennsylvania State University.

⊗ Abstract published in *Advance ACS Abstracts,* July 1, 1996.

(1) (a) Swalen, J. D.; Allara, D. L.; Andrade, J. D.; Chandross, E. A.; Garoff, S.; Israelachvili, J.; McCarthy, T. J.; Murry, R.; Pease, R. F.; Rabolt, J. F.; Wynne, K. J.; Yu, H. *Langmuir* **1987**, *3*, 932−950. (b) For a general review, see: Ulman, A. *An Introduction to Ultrathin Organic Films*; Academic Press: Boston, 1991. (c) Whitesides, G. M.; Ferguson, G. S.; Allara, D. L.; Scherson, D.; Speaker, L.; Ulman, A. *Crit. Rev. Surf. Chem.* **1993**, *3*, 49−65.

(2) Laibinis, P. E.; Whitesides, G. M. *J. Am. Chem. Soc.* **1992**, *114*, 9022−9028.

(3) Lercel, M. J.; Redinbo, G. F.; Pardo, M.; Rooks, M.; Tiberio, R. C.; Simpson, P.; Sheen, C. W.; Parikh, A. N.; Allara, D. L. *J. Vac. Sci. Technol.* **1994**, *B12*, 3663−3667.

(4) (a) Tarlov, M. J.; Burgess, D. R. F., Jr.; Gillen, G. *J. Am. Chem. Soc.* **1993**, *115*, 5305−5306. (b) Huang, J.; Hemminger, J. C. *J. Am. Chem. Soc.* **1993**, *115*, 3342−3342.

(5) Kumar, A.; Biebuyck, H. A.; Abbott, N. L.; Whitesides, G. M. *J. Am. Chem. Soc.* **1992**, *114*, 9188−9189.

(6) (a) Allara, D. L.; Nuzzo, R. G. *Langmuir* **1985**, *1*, 45−52 and 52−65. (b) Sondag, A. H. M.; Raas, M. C. *J. Chem. Phys.* **1989**, *91*, 4926−4931.

(7) Schlotter, N. E.; Porter, M. D.; Bright, T. B.; Allara, D. L. *Chem. Phys. Lett.* **1986**, *132*, 93−98.

(8) Tao, Y. T. *J. Am. Chem. Soc.* **1993**, *115*, 4350−4358.

(9) Tao, Y. T.; Ma, L. F. *J. Chin. Chem. Soc.* **1994**, *41*, 481−485.

S0002-7863(96)00672-5 CCC: $12.00

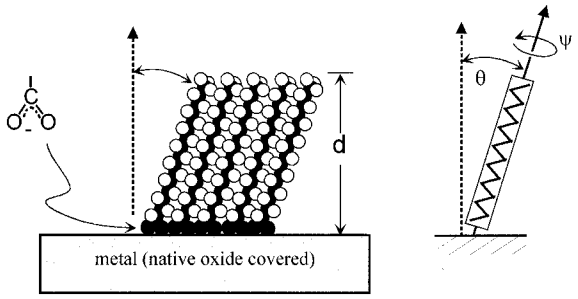

Figure 1. Schematic representation of a monolayer self-assembled from a long-chain *n*-alkanoic acid onto ambient Ag, Cu, or Al surfaces. The adjacent diagram defines the tilt angle, θ, of the chain axes from the surface normal and the twist angle, ψ, which characterizes the rotation of the C−C−C zigzag plane out of the plane defining θ.

surface region. The time-dependent structural rearrangements were analyzed by IRS and liquid drop contact angle measurements. The results show that HCl molecules can readily penetrate and disrupt the chain organization in these dense SAMs in a manner very dependent on the specific substrate metal. In particular, for the case of Ag, the molecular packing is radically disrupted in a process which rearranges the initially uniform, quasi-two-dimensional array of RCO_2^- species (R ≡ alkyl) to dispersed, nanometer-scale size islands of RCO_2H crystallites. Further, a surprising surface mobility of the molecular chains is shown by the nearly reversible formation of the original planar SAM from the 3-dimensional island structure upon standing for extended times under ambient conditions.

2. Experimental Section

1. Materials. The *n*-alkanoic acids of various chain lengths used were obtained from Merck, Tokyo Chemical Industry Co., and Aldrich. Purification was done by distillation or recrystallization from ethanol, as appropriate. Sodium *n*-hexadecanoate and anhydrous hydrogen chloride (99%) were obtained from Aldrich and used without further purification. Hexadecane, used both as the self-assembly solvent and the contact angle liquid, was dried by percolation twice through activated alumina. Silver, copper, and aluminum metals (99.99%) were obtained from Johnson Matthey.

2. Monolayer Preparation and HCl Exposure. The preparation of the evaporated metal substrates and the procedure for monolayer adsorption from hexadecane solution have been previously described.[8] Exposure of the samples to HCl vapor was carried out by placing the sample (1) in the vapor above several drops of concentrated hydrochloric acid in a beaker or (2) in a controlled atmosphere chamber, flushed with high-purity nitrogen followed by introduction of anhydrous HCl vapor, maintained at 0.01 atm of partial pressure, from a syringe. In the latter case, after an appropriate exposure time, usually 10 s, the chamber again was flushed with nitrogen. For studies of reversibility, the HCl-exposed samples were placed in a clean chamber maintained at 25 °C and removed periodically for characterization.

3. Infrared Spectra. External reflection spectra were taken with a Bomem MB-100 Fourier transform spectrometer equipped with a liquid nitrogen cooled mercury cadmium telluride (MCT) detector. The incident infrared beam was fixed at an 86° angle of incidence and adjusted to *p*-polarization through a wire-grid polarizer. The sample and detector optics were located in an external optical bench immediately following the interferometer exit. The final spectra were obtained by co-addition of 1000 scans collected at 2-cm^{-1} resolution. The spectral intensities are reported as $-\log(R/R_o)$ where R and R_o are the reflectivities of the sample and a clean gold-coated wafer, respectively. Details of the optics and spectral methods are described elsewhere.[10] Transmission spectra of solid-phase *n*-alkanoic acids dispersed at known concentrations in KBr pellets were taken on a Mattson-Research Series Fourier transform spectrometer equipped with a medium band pass MCT detector and operating at 2-cm^{-1} resolution. The KBr pellet spectra were used to determine the complex optical function spectra defined as,

$$\hat{n}(\nu) = n(\nu) + ik(\nu)$$

where n and k are the real and imaginary parts of the refractive index, and n is the spectral frequency. The methods for this calculation are described in detail elsewhere.[11]

These optical functions were used as inputs to simulations of the observed reflection spectra. For this purpose, the scalar function $\hat{n}(\nu)$ was converted to a tensor quantity, $\tilde{\mathbf{n}}(\nu)$, in order that the orientation of the adsorbates on the surface could be specified properly. The procedure has been described elsewhere,[11] but briefly it consists of first evaluating the tensor elements $n_{ij}(\nu)$ by decomposing the scalar $k(\nu)$ spectrum into individual oscillators (modes), using curve resolution as necessary. The result for hexadecanoic acid is shown in Figure 2 where the C−H and O−H stretching modes of the CH_3, CH_2, and OH groups have been resolved into individual k bands. The descriptions of these specific modes are given in Table 1. Next, the transition dipole moment of each oscillator is assigned a direction relative to the molecular coordinate system and finally the k intensity of each oscillator is appropriately scaled to account for the differences in the transition moment directions. Once the connection between the molecular and laboratory (SAM sample and spectrometer) coordinate frames is made, the orientation of the molecule on the surface is described in terms of the orientations of each oscillator transition dipole as specified by a specific spectrum of tensor elements ($n_{ij}(\nu)$) which includes all the transitions of interest. Changes in the molecular orientation then can be specified as needed by application of a 3 × 3 rotation matrix.

The spectral simulations were carried out using previously developed methods[11] in which the monolayer structures are modeled as collections of uniformly oriented chains arranged in a parallel layer on a planar substrate. All the simulations in the present study were based on 3-medium models consisting of ambient(air)/SAM/metal. The presence

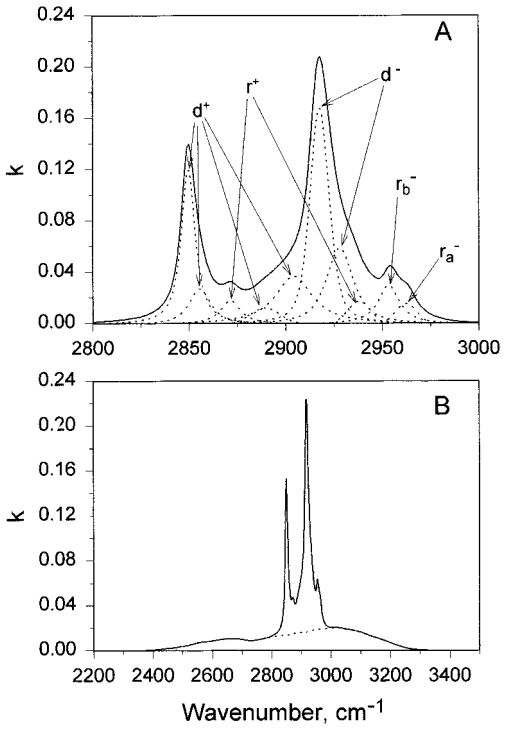

Figure 2. Isotropic *k* spectrum of bulk polycrystalline *n*-hexadecanoic acid. The dotted lines indicate the resolved components assigned to individual vibrational modes: (A) the isolated C−H stretching modes and (B) the total spectrum including both the C−H and O−H stretching modes with the hydrogen bonded O−H stretching mode contribution shown by the dotted line.

(10) Laibinis, P. E.; Whitesides, G. M.; Allara, D. L.; Parikh, A.; Tao, Y. T.; Nuzzo, R. G. *J. Am. Chem. Soc.* **1991**, *113*, 7152.

(11) Allara, D. L.; Parikh, A. N. *J. Chem. Phys.* **1992**, *96*, 927−945.

Table 1. Observed Infrared Spectral Peak Frequencies and Mode Assignments for a Self-Assembled Monolayer (SAM) of *n*-Hexadecanoic Acid on Ag, before and after Treatment with HCl Vapor, and for Reference Compounds Dispersed in KBr Matrices

	peak positions for different forms of *n*-hexadecanoic acid, cm^{-1}				
vibrational mode[a]	polycrystalline acid	polycrystalline sodium salt	SAM/Ag	SAM/Ag, after HCl treatment	ref
OH str (H-bonded)	2500−3400 (br)				22
asym CH_3 str (ip); r_a^-	2962.8		2962.9	2962.5	13, 15
asym CH_3 str (op); r_b^-	2954.2	2955.4		2952.8	13, 15
sym CH_3 str, FR; r_{FR}^+		2937.4	2935.9	2932.8	13, 15
antisym CH_2 str (op); d^-	2918.0	2918.4	2915.3−2919.2	2917.1	13, 15
antisym CH_3 str (ip); r^+	2871.4	2873.4	2876.6		13, 15
sym CH_2 str (ip), d^+	2850.0	2850.0	2849.1	2848.1	13, 15
C═O str (H-bonded)	1702.4			1701.5	20, 21
antisym CO_2^- str		1559.5			13, 21
sym CO_2^- str		1422.6, 1445.3	1401.2		13, 21
asym CH_3 def	*b*			1456.9	23
CH_2 HCH bend	1463.9, 1471.9	1463.7, 1469.7	1470.1	1463.1, 1471.7	21−26
$C_\alpha H_2$ HCH bend + other modes?	1410.9			1411.8	20, 21, 23
[C-O str] + [COH def]	∼1300, 1430.8			∼1300, 1430.3	20
CH_3 def	1384.1	1381.6	1382.4		23
CH_2 (wag + twist)	1349.3, 1329.8, 1311.4, 1295.5, 1272.1, 1250.8, 1228.8, 1208.4, 1187.8	1339.8, 1322.6, 1301.1, 1278.3, 1255.5, 1233.4, 1210.9, 1188.8	1350.6, 1334.9, 1316.9, 1296.4, 1275.4, 1253.7, 1232.1, 1210.2,	1347.5, 1329.7, 1308.8, 1294.4, 1272.0, 1250.8, 1228.6, 1208.4, 1188.0	24
OH bend (op, H-bonded dimer)	941.6			942.8	20, 21
CH_2 rock, crystal field split	720.43, 727.65	720.2		720.3, 728.4	22−26

[a] Spectroscopy notations: str = stretch, def = deformation, ip = in plane, op = out of plane, FR = Fermi resonance, asym = asymmetric, antisym = antisymmetric, sym = symmetric. [b] Poorly resolved feature.

of non-metallic layers, e.g., native oxide or metal chloride layers, on the metal substrate was ignored for purposes of the calculations. The errors inherent is this approximation, in terms of the changes in spectral intensities, are within 1%, as determined by additional simulations based on appropriate 4-medium models using appropriate values of the optical functions of the non-metallic layers.

4. Contact Angle and Other Measurements. Contact angle measurements were made with hexadecane and water using a Rame-Hart NRL Model 100 goniometer. A minimum of three independent measurements were made for each sample. The static angles are reported and are the average of more than three batches of samples. Typical sample-to-sample errors are within ±2°. Ellipsometry measurements, used as an occasional check of coverage, were made at 632.8 nm using a null ellipsometer set at a 70° incidence angle. The standard approach using a psuedodielectric function derived from a freshly evaporated metal film was followed and an isotropic refractive index value of 1.47 was assigned to the monolayer film. Details can be found elsewhere.[6] X-ray photoelectron measurements, used to check the surface chemistry of the HCl/Ag reaction, were carried out on an in-house customized Hewlett Packard 5950A spectrometer using monochromatized Al (Kα) radiation (1486.6 eV), a multichannel resistive anode detector, and the sample tilt set to fix the electron takeoff angle at 38.5° with respect to the sample surface plane.

3. Results

1. Monolayers on silver. A. C16 SAMs. i. Unexposed SAM Structure. The major effort in examining SAMs on Ag surfaces was concentrated on the SAM prepared from $C_{15}H_{31}CO_2H$, designated for convenience as the C16/Ag SAM. The typical monolayer thickness of the C16/Ag SAM system was determined by single wavelength ellipsometry to be 21 ± 1 Å. This film surface showed advancing contact angles of 54 and 110° for hexadecane and water, respectively, with corresponding hystereses of <10 and <15°, respectively. These contact angle values correspond to the high side of the range of ones reported for a variety of different long-chain alkyl SAMs with near-normal orientation of chains, e.g., octadecylsiloxanes on SiO_2 surfaces,[12] and signify that the alkyl chains are densely packed with a pure CH_3 ambient surface.

The observed IRS spectra for the C16 SAM, both before and after interaction with HCl vapor, are given in Figure 3. The

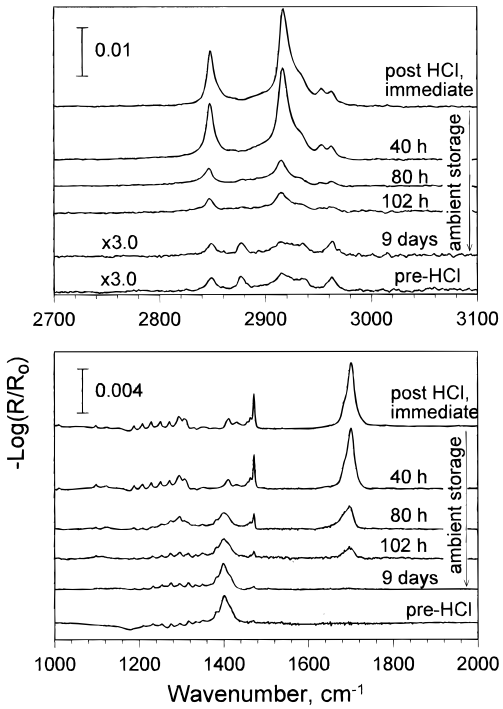

Figure 3. External reflection spectra of a *n*-hexadecanoic acid monolayer on Ag before and after a 10-s HCl vapor exposure. The post-exposure spectra were taken (1) immediately after removal from the HCl vapor and (2) after storage in ambient air in a closed container at ambient temperature for periods of 40 h, 80 h, 102 h, and 9 days. The intensities of the pre-HCl exposure and the 102-h storage spectra are multiplied by 3 for presentation of detail.

observed frequencies are given in Table 1 along with those obtained from the transmission spectra of the bulk polycrystalline acid and its sodium salt, shown in Figure 4. Interpretations of most aspects of the initial SAM (pre-HCl exposure) spectrum can be found elsewhere[13] and consequently are not presented here in detail. Rather, only those features of particular interest in analyzing the subsequent effects of HCl vapor on the monolayer structure are examined. In accordance with the earlier work (see also Table 1),[13] the present spectra indicate

(12) Maoz, R.; Sagiv, J. *J. Colloid Interface Sci.* **1984**, *100*, 465−496.

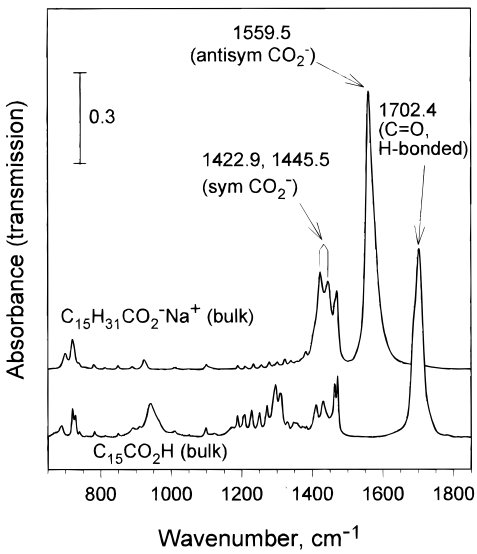

Figure 4. Transmission spectra of bulk *n*-hexadecanoic acid and its sodium salt dispersed in KBr matrices.

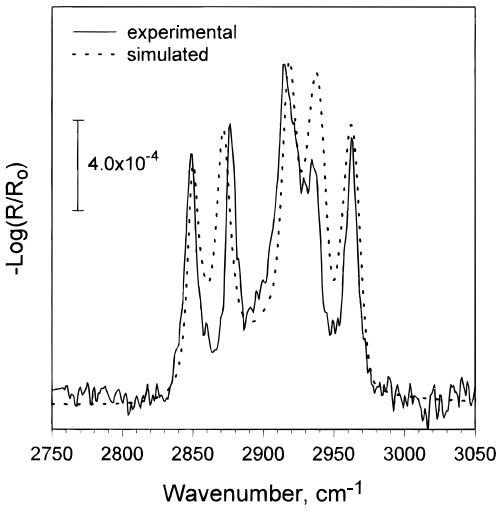

Figure 5. Experimental and simulated C−H stretching region reflection spectra for a *n*-hexadecanoic acid SAM on Ag. The simulated spectrum, shown by a dotted line, represents a best fit to experimental data and was calculated using θ and ψ values of 19.5 ± 2 and 46 ± 1°, respectively (angles defined in Figure 1).

that the initial C16 SAM consists of (1) close packed chains in a highly *trans* conformation, primarily established by the series of sharply defined wag/twist modes between 1150 and 1350 cm^{-1}, (2) completely dissociated protons on the CO_2H groups as indicated by the absence of the C═O stretching mode absorption of the CO_2H group together with the appearance of the intense peak at 1401 cm^{-1} assigned to the symmetric C−O stretching mode of the $-CO_2^-$ moiety, and (3) placement of the symmetrical (C_{2V} point group) $-CO_2^-$ group at the substrate surface with both O atoms nearly equidistant from the surface, as indicated by the near-zero intensity of the antisymmetric C−O stretching mode. Quantitative spectral interpretations are made below for the high frequency C−H stretching modes. However, the intensities of the low-frequency modes were not treated quantitatively since the chain and carboxylate group mode features are overlapped to a large degree and bulk model compounds could not be found which simultaneously could give suitably accurate optical functions for both the SAM carboxylate and chain modes.[14]

Figure 5 shows the detailed C−H stretching mode features of the CH_2 and terminal CH_3 groups in the unexposed SAM. Mode assignments are given in Table 1.[15] This experimental spectrum was simulated using a 3-medium model air/SAM/Ag in which the SAM optical function spectra (tensor formulation) were based on the values shown in Figure 2A which were derived from transmission spectra of bulk polycrystalline samples of n-$C_{15}H_{31}CO_2H$ dispersed in KBr. The optical constant function for the evaporated Ag film substrate was obtained by interpolation of values from the literature.[16]

The initial simulations were performed using a single-chain model consisting of a uniform array of all-*trans* C16 chains with orientations defined by the tilt and twist angles θ and ψ, defined in Figure 1. These angles were varied and a best fit to the experimental d^+ and d^- bands was achieved with θ and ψ values of 19 ± 2 and 44 ± 1°, respectively. While these $d^\pm$ fits are very close, the corresponding fits to the CH_3 bands were in error by ∼15%. Some disagreement is to be expected since at room temperature a degree of conformational disorder in the chain termini is likely, thus leading to a distribution of CH_3 group orientations.[17]

A two-chain model was considered next. Precedent for this type of structure is based on the fact that the common crystalline form of bulk-phase *n*-hexadecanoic acid exhibits an orthorhombic subcell with a setting angle of 90° between the two C−C−C planes,[19] and on the reported conclusion that the C20 SAM on Ag consists of an orthorombic type of subcell structure.[7] The single-chain model result of $\psi = 44 \pm 1°$ corresponds to that expected for an orthorhombic type of subcell packing in which the average of the individual chain values of ψ is always 45° for any subcell orientation. The two-chain simulations were performed using a model with the angle between the C−C−C planes varied in a small region around 90°. These results, shown in Figure 5, show a best fit for $\theta = 19 \pm 2°$, identical to the single-chain value within experimental error, with a subcell chain setting angle of 90 ± 1°. This value of θ is centrally located within the range of tilt angles reported for long-chain *n*-alkanoic acids/Ag: 10−17°, Schlotter *et al.*;[7] 15−25°, Tao;[8] and 26−28°, Samant *et al.*[18] However, compared to the single-chain model, the fit is slightly improved (∼5% error) as judged by closer fitting of the CH_3 modes except for the high-frequency component of the r_{FR}^+ mode (∼2936 cm^{-1}). The difficulty in obtaining a complete fit of the CH_3 C−H stretch modes suggests

(13) See refs 7 and 8 and: (a) Smith, E. L.; Porter, M. D. *J. Phys. Chem.* **1993**, *97*, 8032−8038. (b) Ahn, S. J.; Son, D. H.; Kim, K. *J. Mol. Struct.* **1994**, *324*, 223−231.

(14) The intensities, frequencies and line widths of the $-CO_2^-$ modes are well-known to be highly dependent on their ionic environment and thus the specific environment at the $-CO_2^-$/Ag interface cannot be accurately represented with analogous bulk carboxylate salts. In addition, we continually observe that the chain packing in *n*-alkanoate salts is poorer than in the corresponding SAMs, thus limiting the use of these salts as a source of accurate optical function values for simulation of SAM spectra. However, the spectra of the bulk long-chain acids in the C−H stretching region exhibit an extremely close match of frequencies and line widths to the corresponding SAMs. For this reason, the optical functions obtained from the bulk acids were used for quantitative simulations of the non-carboxyl features of the SAM spectra. Tabulated optical constant data of a number of the carboxylic acid and alkali metal salts are available from one of the authors (D.L.A.) on request.

(15) Infrared band assignments for the C−H stretching modes of *n*-alkyl chains can be found in numerous references, e.g.: MacPhail, R. A.; Strauss, H. L.; Snyder, R. G.; Elliger, C. A. *J. Phys. Chem.* **1984**, *88*, 334−341. Previous assignments in SAMs can be found elsewhere, e.g., refs 6a, 7, 10, and 11.

(16) Palik, E. D. *Handbook of Optical Constants of Solids*; Academic Press: New York, 1985; pp 353−357.

(17) Such effects are prevalent in other SAM systems, e.g., *n*-alkanethiolates on Au (ref 10).

(18) Samant, M. G.; Brown, C. B.; Gordon, J. G., II *Langmuir* **1993**, *9*, 1082−1085.

(19) (a) Verma, A. R. *Proc. R. Soc. A* **1955**, *228*, 34−50. (b) Sydow, E. V. *Arkiv Kemi.* **1956**, *9*, 231−254.

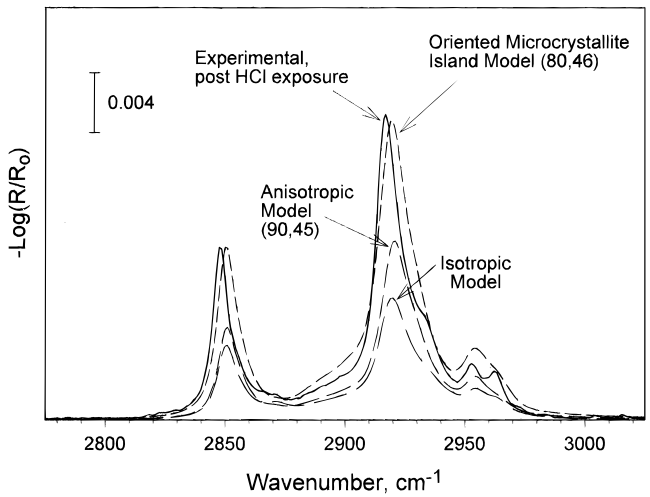

Figure 6. Experimental C−H stretching region spectrum of a *n*-hexadecanoic acid monolayer on Ag after exposure to HCl vapor for 10 s. The spectrum was taken immediately after the sample had been removed from the HCl vapor. Also shown are simulated spectra based on three proposed, post-HCl-treatment film structures. The details of these structures are given in the text.

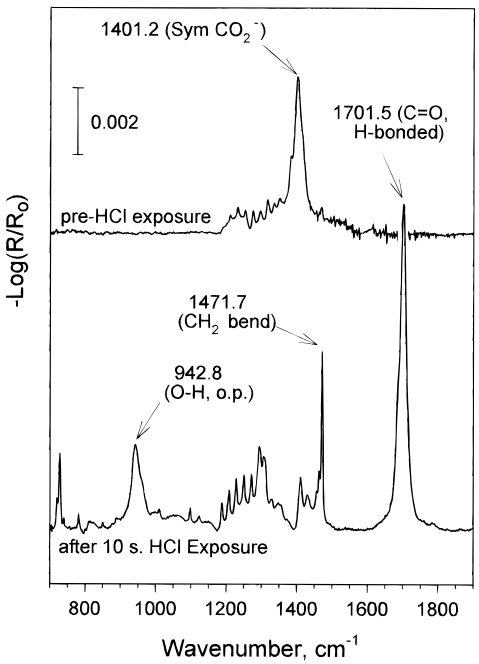

Figure 7. Experimental low-frequency-region spectrum of a *n*-hexadecanoic acid monolayer on Ag before and after 10-s exposure to HCl vapor. The spectrum was taken immediately after the sample had been removed from the HCl vapor.

that there are slight differences in the nature of the Fermi resonance interaction in the bulk polycrystalline C16 sample and the SAM.

ii. HCl Exposed SAM Structure. (a) Qualitative Interpretations. Exposure of the monolayer sample to HCl vapor, from either the concentrated acid or the anhydrous vapor (see Experimental Section), gave IRS and wetting results independent of the HCl source. However, for purposes of systematic comparison, the procedure of exposure to 0.01 atm of HCl vapor in a chamber (see Experimental Section) was adopted as the standard method.

Upon exposure, for even as little as 10 s, dramatic changes were observed in both the IRS spectrum and the wetting behavior. The water contact angle decreased from 110 to ∼70° and hexadecane completely wetted the sample. The IRS spectrum, taken immediately after HCl exposure, is given in Figure 3; the observed peak frequencies with corresponding assignments are given in Table 1.

In the high-frequency region, the most striking change is the ∼15-fold increase in the CH_2 stretching mode intensities relative to the unexposed film spectrum. In contrast, the corresponding peak positions remain nearly unchanged at 2848 and 2917 cm^{-1} for d^+ and d^-, respectively, an indication that the chains maintain high conformational ordering. With regard to the CH_3 C−H stretching modes, the symmetric r^+ signature, prominent in the unexposed SAM spectrum at 2876 cm^{-1}, has nearly disappeared while the r_b^- out of plane asymmetric feature, absent in the unexposed film, is now clearly observed at 2953 cm^{-1}. The C−H stretching region of the C16/Ag SAM exposed to HCl vapor for 10 s is shown in detail in Figure 6. The low frequency region of the C16/Ag SAM spectrum before and after HCl exposure is shown in detail in Figure 7. These spectra reveal changes in both the carboxyl moiety and the alkyl chains. These are discussed in order.

The most readily observed changes are seen in the low-frequency region (Figure 7), exemplified by the disappearance of the $-CO_2^-$ stretching mode feature, present at 1401 cm^{-1} in the initial SAM, and the appearance of the CO_2H stretching mode feature at 1701.5 cm^{-1}, absent initially. This change establishes that protonation of the $-CO_2^-$ group has occurred to form the original acid molecule. A comparison of the low-frequency spectra of the bulk, polycrystalline C16 acid and the HCl-exposed SAM (Figures 4 and 7, respectively) reveals nearly identical matches of the frequency positions and line widths of the spectral features. Since the structure of crystalline hexadecanoic acid is known to be monoclinic[19] with the all-*trans* chains arranged in head to head, hydrogen-bonded dimers, *viz*.,

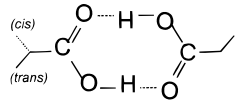

one can conclude that the HCl-exposed SAM also possesses this structure. Further support for the dimer structure is given by the appearance of a strong peak at 942 cm^{-1}, characteristic of the out-of-plane O−H bending mode in the acid dimer.[20] Additionally, the absorption near 1300 cm^{-1} (overlapping the chain twist/wag progression bands) is characteristic of the coupled C−O stretch and the in-plane O−H deformation of the hydrogen-bonded CO_2H moiety in the *trans* configuration (see diagram above).[20,21] This configuration is the only one observed at liquid helium temperatures, where it is the lower energy form by ∼0.2 kcal/mol for even-numbered (C8−C20) acids. At room temperature it represents approximately 25% of the total population.[20]

Table 1 shows that all of these features match in detail with those observed in the spectrum of polycrystalline hexadecanoic acid. One distinct difference, however, is the absence of the O−H stretching mode absorption in the HCl-exposed SAM. This absorption occurs as an extremely broad and distinct feature in the 2400−3200-cm^{-1} region for hydrogen-bonded carboxylic acids in solid and liquid forms (see Figure 2B).[22] The absence of this signature in the SAM spectrum is attributed to an orientational effect in which the acid dimer ring lies nearly parallel to the substrate surface. Since the transition dipoles

(20) Hayashi, S.; Umemura, J. *J. Chem. Phys.* **1975**, *63* (5), 1732−1740.
(21) Bellamy, L. J. *The Infrared Spectra of Complex Molecules*; Wiley: New York, 1975.
(22) Sinclair, R. G.; McKay, A. F.; Jones, R. N. *J. Am. Chem. Soc.* **1952**, *74*, 2570−2575.

associated with the O−H stretching modes in the dimer ring are parallel to the ring plane, the electromagnetic selection rules[11] require that this mode intensity diminish as the ring aligns increasingly parallel to the metallic substrate surface. Calculations of this effect will be discussed in the next section.

The match of the alkyl chain mode features of the HCl-exposed SAM and the monoclinic bulk acid,[23] as seen in Figures 4 and 7, shows that the chain arrangements must be quite close, if not identical. First, the exact match, within the spectral resolution, of the frequencies of the component peaks of the two coupled twist and wagging mode series shows that the alkyl chains in the two forms exhibit essentially all-*trans* conformational ordering.[24] Second, the observation of the CH_2 bending and rocking modes in the exposed SAM at 1463.1 and 1471.7 cm^{-1} and 720.3 and 728.4 cm^{-1}, respectively, nearly identical to the positions in the crystalline acid spectrum, supports the same orthorhombic subcell packing as in the bulk crystals.

One difference between the SAM and bulk crystalline acid spectra, however, is that in the SAM spectrum there is a skewing in the relative intensities of the component peaks of the CH_2 bending and rocking modes to favor the higher frequency component in each pair. This observation can be due to a combination of electromagnetic orientation effects,[11] related to the polarization directions of the split oscillators in the **a**,**b** crystal plane,[25,26] and their intrinsic oscillator strengths ($\propto k(\nu)$). Since these effects cannot be easily separated at present, a quantitative interpretation is difficult.[27] One can also consider that the doublet intensity skewing arises from the presence of a small component of triclinic crystallites with singlet CH_2 rocking and bending modes which could contribute some additional intensity in the vicinity of the high-frequency doublet components of the monoclinic material. However, this possibility can be discounted since all other spectral features of the HCl-exposed SAM match so closely with the monoclinic bulk spectrum. Further, the HCl-exposed SAM spectrum shows a doublet CH_2 rocking mode near 720 and 728 cm^{-1}, typical locations for *n*-alkanoic acids with orthorhombic subcell packing,[28] whereas the location of this mode for a triclinic structure is observed in the case of *n*-tridecanoic acid to be a singlet at ∼716 cm^{-1}.[29]

(b) Quantitative Interpretations. The IRS data of the HCl-exposed C16/Ag SAMs were analyzed quantitatively by performing spectral simulations based on different models representing possible structures of the films. The major effort was placed in the high-frequency region spectra where the individual mode features can be better resolved and transition moment directions more easily assigned than in the low-frequency region. The calculations were carried out using the tensor elements ($n_{ij}(\nu)$) generated from the isotropic $\hat{n}(\nu)$ spectrum of the polycrystalline C16 acid. Figure 2A shows the $k(\nu)$ portion of the $\hat{n}(\nu)$ spectrum with the contribution from the broad O−H stretching mode, visible in Figure 2B, subtracted out. Since no broad O−H feature was observed in the experimental spectrum (see Figures 3 and 6), the C−H mode simulations were simplified by using the $\hat{n}(\nu)$ optical function spectrum with the O−H feature removed. Later, this feature was included to probe the orientation of the $-CO_2H$ dimer moiety. Four limiting models were considered in which protonation of the initial $-CO_2^-$ moiety produces adsorbed C16 acid molecules existing as (1) a uniform, random (isotropic) monolayer of crystalline molecules, (2) a uniform, anisotropically oriented ensemble of adsorbates with a uniform chain tilt and twist, (3) isolated islands of microcrystallites with uniform crystallite sizes and random orientations (isotropic), or (4) isolated islands of microcrystallites with uniform crystallite sizes and uniform orientations. The simulations based on the heterogenous density distribution in models 3 and 4 were carried out by applying an effective medium approximation (EMA) to the determination of the SAM layer optical function spectra. In this approximation, the SAM media were considered to be uniform mixtures with variable volume fractions of void regions and C16 acid crystallites. In view of the limited number of molecules per unit area in the SAM (∼5 per nm^2), the sizes of the crystallites were assumed to be well below the wavelength of the infrared probe light, thus eliminating the necessity of applying scattering corrections. In carrying out the calculations, the thickness of the SAM layer was defined as the line across the tops of the uniform-sized crystallites. The effective optical function tensors of these SAM films were then calculated on the basis of the Bruggeman equation:

$$\sum_{i=1}^{n} f_i \left(\frac{\epsilon_i - \epsilon}{\epsilon_i + 2\epsilon} \right) = 0$$

where n is the total number of components in the multiphase system, f_i and ϵ_i are the volume fraction and dielectric constant, respectively, of the ith component, and ϵ is the effective dielectric constant of the multiphase layer.[30,31] The details of the application of the EMA to the simulation of IRS spectra will be presented elsewhere.[32]

The results of the C−H mode simulations are shown in Figure 6 where it can be seen that only model 4 gives satisfactory fits

(23) Hill, I. R.; Levin, I. W. *J. Chem. Phys.* **1979**, *70* (2), 842−851.

(24) (a) Snyder, R. G.; Schachtschneider, J. H. *Spectrochim. Acta.* **1963**, *19*, 85−116. (b) Sinclair, R. G.; McKay, A. F.; Jones, R. N. *J. Am. Chem. Soc.* **1952**, *74*, 2575−2578.

(25) Snyder, R. G. *J. Mol. Spectrosc.* **1961**, *7*, 116−144.

(26) Susi, H. *J. Am. Chem. Soc.* **1959**, *81*, 1535−1540.

(27) Electromagnetic orientation effects will arise since the transition moment directions of each component of the two doublets are mutually orthogonal; thus their intensity ratio will modulate as a function of the crystal unit cell orientation to the polarization of the exciting IR electric field, essentially perpendicular to the substrate plane for the present case of grazing angle incidence on Ag. In particular, since the higher frequency components at ∼1472 and ∼728 cm^{-1} in the doublet CH_2 bending and rocking modes, respectively, are parallel to the ***a*** axis while the low frequency components are parallel to the ***b*** axis (refs 25 and 26), the relative doublet intensities will be determined by the ***a***, ***b*** plane surface alignment. In the present example of the C16/Ag SAM spectrum taken after 10 s of HCl exposure (Figure 7) the high/low frequency mode intensity ratios for both the CH2 rocking and bending modes are ∼2.5:1. This result suggests that the **a**,**b** plane is oriented preferentially with the **a** axis away from the surface. However, without a knowledge of the intrinsic oscillator strengths this conclusion must be considered speculative.

(28) Barr, M. R.; Dunell, B. A.; Grant, R. F. *Can. J. Chem.* **1963**, *41*, 1188−1196.

(29) The triclinic form of *n*-hexadecanoic acid is apparently difficult to form but can be formed readily for *n*-tridecanoic acid by crystallization from ethanol at 0 °C (ref 19b). Following this procedure, C13 acid triclinic crystallites were prepared and a transmission IRS spectrum taken for a KBr dispersion. The rocking mode peak was observed as a singlet at 716 cm^{-1}. [Hietpas, G. D.; Allara, D. L. Unpublished results.]

(30) (a) Bruggeman, D. A. G. *Ann. Phys.(Leipzig)* **1935**, *24*, 636. (b) Aspnes, D. E. *Thin Solid Films* **1982**, *89*, 249−262. (c) Jellison, G. E., Jr. *Thin Solid Films* **1993**, *234*, 416−422.

(31) We note that more rigorous treatments are available for calculations of the effective local electromagnetic field strengths in heterogeneous thin film media than the one used here [for example, see: Beaglehole, D. *Mater. Res. Soc. Symp. Proc.* **1995**, *366*, 77−88]. In general, deviations from the accuracy of EMA treatments based on uniform dielectric functions for the constituent materials in a thin heterogeneous slab will arise for films comprised of monolayers of particles on the size scale of ∼10 nm or less, with the exact deviations highly dependent on the size of the bulk dielectric function. However, since these deviations will primarily arise from the screening effects of in-plane (surface) polarization fields, they then will be neglible in the cases of highly metallic substrates, such as the present case, where the in-plane electric fields are near vanishing. For this reason, and also because of the overall uncertainty of the exact sizes of the crystallites and their distributions (see ref 33) the present level of calculations using standard EMA theory was selected as appropriate for the data analysis. More detailed approaches will be described elsewhere (see ref 32).

(32) Hietpas, G.; Parikh, A.; Allara, D. Manuscript in preparation.

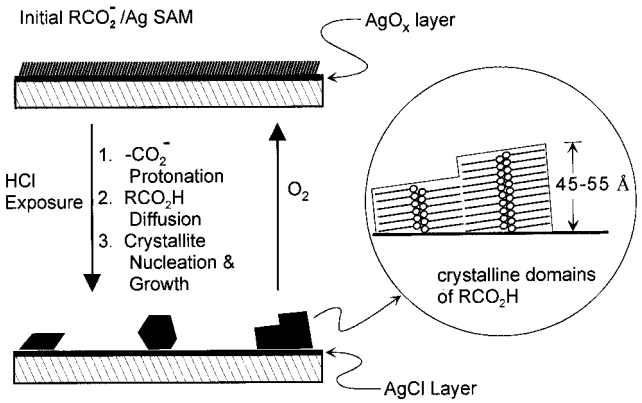

Figure 8. Schematic representation of proposed structures for a *n*-hexadecanoic acid monolayer on Ag before and immediately after a 10-s HCl exposure.

to the experimental data. Model 1 for an isotropic monolayer is not only physically unrealistic (the chains are known to be oriented) but fails completely to match the experimental intensities by a factor of ∼2.5. The addition of anisotropy through application of model 2 also fails to match intensities, regardless of the value of θ selected over the entire range of 0−90°; the closest fit occurs at 90° but is still extremely poor. Simulations based on model 3 fail, regardless of the volume fraction of crystallites chosen, showing that the film is not optically isotropic, i.e., the crystallite orientations are not random. Good fits to the experimental spectra were obtained using model 4 for heterogenous SAM structures consisting of uniformly distributed C16 acid crystallites with sizes up to 50 (±7) Å, with uniform orientation of the ***c*** (chain) axes at 80 ± 10° to the surface normal and with an average chain twist ψ of 46 ± 1°.[33] This orientation essentially places the {010} or {100} surface planes in contact with the substrate. Based on the results of this simulation and the monoclinic crystalline structure (see above), a cartoon representation of the final types of crystallite structures is shown in Figure 8.

The C16 acid nanocrystallite structure deduced above places the central rotational symmetry axis of the $-CO_2H$ dimer rings nearly parallel to the substrate surface. Since the transition moment dipole for the O−H stretching mode, $\vec{p}_{OH}$, is in the plane of the dimer ring and parallel to the C−CO_2H bond (see dimer structure given earlier), the $\vec{p}_{OH}$-alkyl-chain axis angle must be ∼18°.[34] In order to test this aspect of the structure, simulations were performed using the $\hat{n}(\nu)$ spectrum with the O−H stretching mode feature included (Figure 2B). These results showed that the O−H stretching peak intensity falls below the experimental noise for alkyl chain tilt values >70° and thus supports the proposed picture with the alkyl chains aligned nearly parallel to the substrate surface. As a further test, these best-fit conditions were applied to simulations for the 942-cm^{-1} out-of-plane O−H bending mode of the acid dimer. Since the appearance of this mode is relatively isolated from neighboring features, the $\hat{n}(\nu)$ spectrum is readily obtained from transmission spectra. The corresponding tensor elements were generated on the basis that the transition moment is perpendicular to the dimer ring plane. Using $\theta = 80°$ for the alkyl chains and an average island size of 50 Å, determined above from the best-fit to the C−H spectrum, simulations were made of the 942-cm^{-1} mode peak in which the only free parameter remaining is the dimer ring rotation about the C−CO_2H bond. The best fit to experiment occurs for a dimer ring twist of 46 ± 2° in a single-chain model, or equivalently, an ∼90° setting angle between the ring planes for a two-chain model. Since the dimer ring plane is fixed parallel to the C−C−C alkyl chain plane, the predicted chain twist is also given by these values. This value is in quantitative agreement with the chain twist obtained from simulations of the C−H stretching mode spectra in Figure 6 and indicates good self-consistency to the proposed crystallite structure.

iii. Reversibility of the HCl-Exposure Process. The above experimental SAM spectra reproducibly gave the same results provided that the spectra were recorded within a few hours after the HCl-vapor treatment. However, upon standing in the ambient for periods of several hours or longer, the spectra slowly began to change and eventually reverted to those of the original, unexposed SAM, as seen in Figure 3. These results clearly indicate that a time-dependent structural reorganization occurs in which the $-CO_2H$ groups are deprotonated and the acid molecules diffuse to reconstitute the original monolayer. This reorganization took about 1 week to complete, as observed by the IRS data, although the exact time was somewhat dependent on the exposure history of the surface. When the spectra indicated a return to the original monolayer, the original contact angle values were also recovered within experimental error. However, greater hysteresis was observed than for the original SAM, *viz.*, ∼30−40° vs 10−15°, a suggestion of a more imperfect surface texture for the reorganized SAM. In addition, the solvent resistance properties of the reorganized SAM returned to the original behavior shown by the change from complete hexane solubility for the HCl-treated SAM to strong resistance to removal by hexane rinsing, observed also for the original SAM. The near reversibility of this reorganization process is quite striking as shown by the ability of a SAM to undergo repeated HCl-exposure/reorganization cycles, although with a slow sample degradation after a few cycles. This behavior is consistent with the observation that continued exposures of the original SAM to HCl vapor causes the appearance of foggy spots on the surface, an apparent beginning of irreversible Ag corrosion.

2. Effect of Chain Length Variation. Similar reorganization phenomena to those above for the C16/Ag SAM occurred, in general, for C8-C24/Ag SAMs, although differences in the type and extent of structural changes were observed. For acids of C14 and longer, a standard 10 s HCl exposure results in changes quite similar to those observed for the C16 SAM, as seen by comparing the C16 IRS data in Figure 3 with corresponding data in Figure 9 for the C15 (*n*-pentadecanoic acid) SAM. In both cases, the original monolayer spectrum is nearly completely recovered after ambient storage. In addition, the intensities of the r^- and r^+ CH_3 modes continue to exhibit the reported odd−even dependence in both the original and recovered films.[8,13a] This dependence is based on the tilt angle of the chains and the head group−substrate geometry and thus is a sensitive measure of the details of the monolayer structure. For the RCO_2H/Ag SAM system, this tilt angle dependence leads to an all CH_3-exposed surface for even-numbered chains, a partial CH_3-CH_2 surface for the odd-numbered chains, and

(33) Attempts were made to verify the general size and surface distribution of these crystallites by atomic force microscopy (AFM). However, because of the inherent nm-scale roughness of the evaporated Ag substrates and the quality of the available instrumentation, it was not possible in these preliminary measurements to unambiguously identify what features were actually due to deposits of hexadecanoic acid. Further work with more carefully prepared substrates and improved instrumentation is in progress.

(34) This angle was determined from the ***C*** form of stearic acid (ref 19b and references therein). This crystalline form (monoclinic symmetry with orthorhombic packing of the hydrocarbon chains) has been reported to be the only one formed for the even numbered fatty acids when rapidly crystallized from the melt or from solution. Accordingly, it is reasonable to assume that the rapid protonation and reorganization accompanying HCl exposure of the C16 SAM also results in this crystalline form.

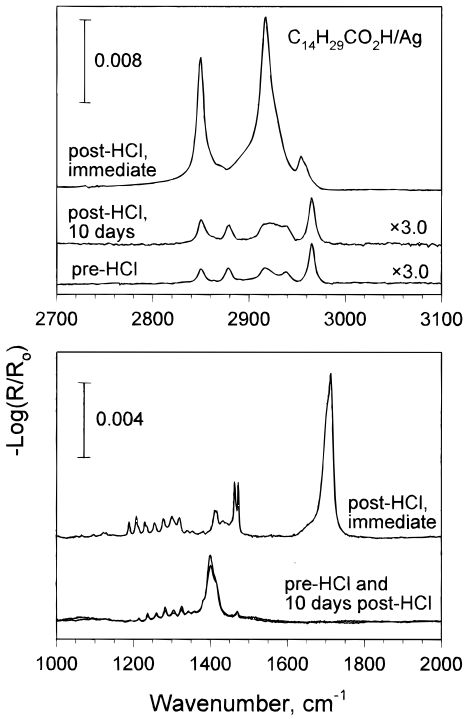

Figure 9. External reflection spectra of a *n*-pentadecanoic acid monolayer on Ag before and after a 10-s HCl-vapor exposure. The post-exposure spectra were taken (1) immediately after removal from the HCl vapor and (2) after 10 days of storage in ambient air in a closed container at ambient temperature. The intensities of the pre-HCl exposure and the 10-day-storage spectra are multiplied by 3 for presentation of detail.

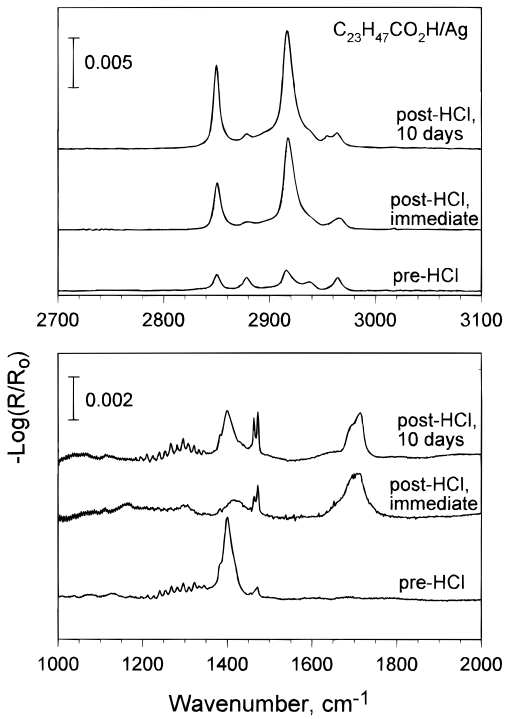

Figure 10. External reflection spectra of a *n*-tetracosanoic acid monolayer on Ag before and after a 10-s HCl vapor exposure. The post-exposure spectra were taken (1) immediately after removal from the HCl vapor and (2) after 10 days of storage in ambient air in a closed container at ambient temperature.

a correlated alternation in the hexadecane wetting properties. The reorganized C15 and C16/Ag SAMs show this structure-sensitive wetting alternation as shown by hexadecane contact angles of 48° and 52°, respectively, identical within experimental error to the original SAM values of 49° and 54°.

As the chain length of the acids increases above C16, the magnitude of the HCl-induced changes gradually diminishes for the same exposure conditions and times. The specific case of the C24 (*n*-tetracosanoic acid)/Ag SAM is shown in Figure 10. For the standard 10-s HCl exposure, the d^+ and d^- mode intensities immediately increase by a factor of 3 or 4, compared to ∼15 for the C16 SAM case, and only a broad, often distorted, C═O stretching mode peak appears near the expected 1701-cm^{-1} frequency for the $-CO_2H$ moiety. Further, the twist/wag progression band, quite prominent in the HCl-exposed C16 SAM spectrum, is no longer present. On standing in the ambient for several days after the initial 10 s exposure, the d^+ and d^- modes continually increase, and after 10 days increase by 100% and 20%, respectively. The progression band returns along with the symmetric $-CO_2^-$ absorption, an indication of partial deprotonation. Increased HCl exposure times, for example, 1 min, result in a fully protonated state, similar to that for C16 acid. Therefore, the state associated with a long-term (10 days) reorganization of the HCl-exposed C24/Ag SAM is likely a state intermediate between the original close-packed monolayer and an agglomeration of microcrystallites observed in the C16 acid/Ag case. Even after 30 days, spectra show the presence of the protonated C24 acid.

As the chain length of the acids decreases from C13 (*n*-tridecanoic acid) and below, HCl exposure results in protonation of the carboxylate groups to form disordered assemblies of the acid molecules. This behavior can be seen in the spectra in Figure 11 for the case of the C12 (*n*-dodecanoic acid)/Ag SAM. After HCl exposure, the d^+ and d^- mode peaks broaden

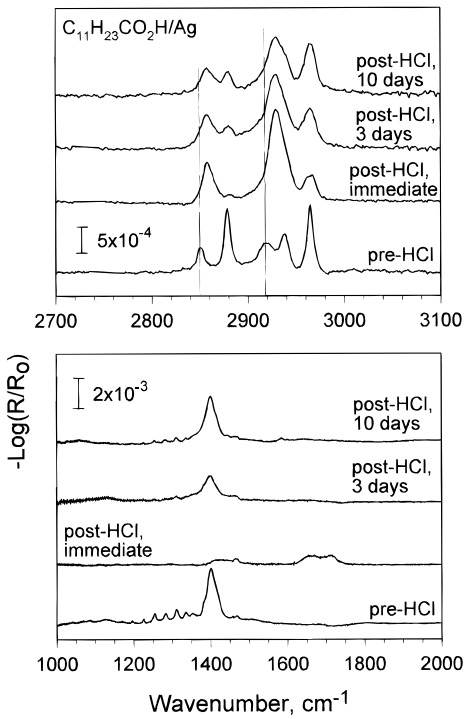

Figure 11. External reflection spectra of a *n*-dodecanoic acid monolayer on Ag before and after a 10-s HCl vapor exposure. The post-exposure spectra were taken (1) immediately after removal from the HCl vapor and (2) after 3 and 10 days of storage in ambient air in a closed container at ambient temperature. The reference lines in the top spectrum show the positions of the d^+ and d^- modes in the pre-HCl SAM.

and shift to ∼2855 and 2928 cm^{-1}, respectively, an indication of strong conformational disordering of the alkyl chains. In the low-frequency region, immediately after HCl exposure, broad, weak features appear between 1650 and 1750 cm^{-1}, and

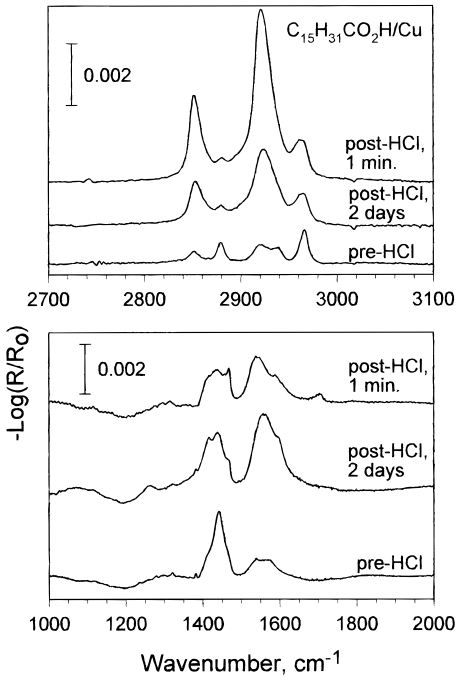

Figure 12. External reflection spectra of a *n*-hexadecanoic acid monolayer on Cu before and after a 1-min HCl-vapor exposure. Post-HCl exposure spectra were taken (1) immediately after removal from the HCl vapor and (2) after 2 days of storage in ambient air in a closed container at ambient temperature.

only a very weak feature remains in the vicinity of the original symmetric $-CO_2^-$ stretch and the original wag/twist progression is gone. Taken together, these results indicate formation of a disordered liquid-like film of the C12 acid. Several days after the initial 10-s HCl exposure, the $-CO_2^-$ feature returns and a gradual shifting of intensities in the C−H stretching region is observed, although the bands remain broad. After 10 days of storage, the C−H stretching mode peaks remain broad and are centered at the high values of 2929 and 2857 cm^{-1}, seen easily by the deviations from the reference lines for the pre-HCl frequencies shown in Figure 11. However, while these data clearly indicate the continued presence of chain conformational disorder, a vestige of the wag/twist progression remains to indicate also the presence of conformationally ordered chains. Further, while both the symmetric to antisymmetric $-CO_2^-$ modes are observed, close analysis of the spectrum shows a corresponding intensity ratio of ∼20/1, respectively, which indicates that the C head group surface geometry involves alignment of the axis through both O atoms parallel to the surface. The combination of all these data constrain the structure of this film to be a mixture of both ordered and disordered C12 carboxylate species, with similarly arranged $-CO_2^-$ head groups, with the different species presumably dispersed in discrete regions across the surface.

These results demonstrate that the kinetics of the HCl-induced reorganization process are strongly dependent on the alkyl chain length. In summary, for acids C13 and shorter, ambient exposure of the HCl-exposed films allows a reversion to a carboxylate species but one that is strongly different from that of the original SAM. In contrast, for acids from *n*-tetradecanoic (C14) to *n*-eicosanoic (C20), complete loss of protons and recovery of the original monolayer spectra occur in a week. However, for the extended chain acids, e.g. *n*-tetracosanoic acid (C24), the deprotonation process is considerably slower.

3. Monolayers on Copper. The IRS spectrum in Figure 12 is qualitatively similar to that of the C16 acid/Ag SAM (Figure 3) and indicates a high degree of organization. Although we have not performed a quantitative analysis of these data, inspection of the C−H stretching modes indicates that this spectrum is roughly consistent with a chain tilt angle closer to normal than with the C16/Ag SAM, *viz.*, $\theta < 19°$, and with a $-CO_2^-$ group tipped away from the surface in an asymmetric fashion.[8] Previous work has shown that the RCO_2H/Cu(oxide) chemisorption interactions are complex with the possibilities of multiple monolayer states[35,36] and, for appropriate conditions, formation of multilayers of carboxylate salts.[37] However, in the present case, the IRS spectra and wetting data are consistent with a monolayer of carboxylate species in which the chains are conformationally ordered and aligned nearly perpendicular to the surface.[8]

Using the standard 10-s HCl vapor exposure, which is completely effective in protonation of the C16 acid/Ag SAM, shows little change in the Cu SAM. Increasing the HCl exposure time to 1 min, however, shows definite effects; the low-frequency-region spectrum shows a peak at 1703 cm^{-1} characteristic of the H-bonded $(CO_2H)_2$ moiety, although with markedly lower intensity than the corresponding peak for the C16/Ag SAM (Figure 3), and there is a persistence of symmetric and antisymetric $-CO_2^-$ stretching modes, although the bands are broader and contain several overlapping peaks relative to the initial SAM. These data indicate that either partial protonation of the $-CO_2^-$ groups occurs, but at a slower rate than for the case of the Cu SAM, or that for a 10-s exposure the deprotonation reaction occurs sufficiently rapidly that it is not observable in the infrared measurements. The partial protonation observed for greater exposure times may be a result of more drastic changes on the Cu surface, which were not caused by a 10-s exposure. This hypothesis is supported by the complexity of the carboxylate modes which indicates that the head groups are present in several different orientations and local environments at the Cu(oxide) surface.

Upon storage in ambient conditions, the C16 acid/Cu SAM shows a partial reversion to the original carboxylate SAM. Figure 12 shows that the spectral intensities of the CH_2 stretches decrease and broaden somewhat while the peaks shift slightly toward higher frequencies. The low-frequency-region spectra show a loss of the weak CO_2H stretching feature near 1700 cm^{-1} and complex changes in the structure of the $-CO_2^-$ mode peaks. We note that the process is variable from sample to sample, as shown, for example, by the observation that the intensity of the 1589-cm^{-1} antisymmetric $-CO_2^-$ stretching mode peak varies; in some cases it was hardly observed, while in others it was extremely prominent. Although the exact basis for this behavior is not known, it may be connected with a variation in the character of the ionic interaction with the substrate after HCl exposure. Such changes could strongly alter the orientation of the $-CO_2^-$ moiety which would cause restructuring of the associated bands with intensity modulations. Finally, after sufficient ambient exposure, a carboxylate salt is formed, but with a distinctly different carbonyl absorption from that of the original SAM. The water contact angle on this surface is about 115°, but in contrast to the oleophobicity of the original SAM, the reorganized surface is wetted by hexadecane. Thus, the protonation−deprotonation cycle on Cu does not appear reversible.

4. Monolayers on Aluminum. Figure 13 shows the IRS spectrum of a C16/Al SAM. The spectra of the initial SAM are in good agreement with those in the earlier report.[6a]

(35) Low, M. J. D.; Brown, K. H.; Inoue, H. J. *J. Colloid Interface Sci.* **1967**, *24*, 252−257.
(36) Tompkins, H. G.; Allara, D. L. *J. Colloid Interface Sci.* **1974**, *49*, 410−421.
(37) Gaines, G. L., Jr. *J. Colloid. Sci.* **1960**, *15*, 321.

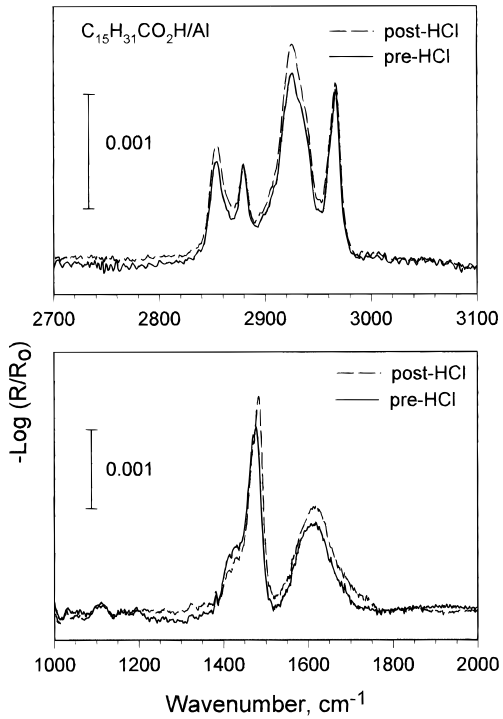

Figure 13. External reflection spectra of a *n*-hexadecanoic acid monolayer on Al before and immediately after a 1-min HCl-vapor exposure.

Exposure to HCl vapor produced no changes in the spectra, even after extended times of 1−3 min. In all cases, the peaks in the C−H stretching region and those due to the $-CO_2^-$ stretching modes remain nearly unchanged indicating a constant chain structure and a lack of protonation of the $-CO_2^-$ head group.

4. Discussion

1. Generalized Reaction Mechanisms. In all cases of the SAMs on the different substrates, highly organized, densely-packed monolayers with oriented alkyl chains are formed, consistent with previous reports. The complex sequence of reaction steps which occur during HCl exposure and subsequent ambient storage of the SAMs in this study are incorporated into the generalized processes 1−4 below.

$$RCO_2^-(\text{2-D, c})/M[\text{oxide}]/M + HCl(g) \rightarrow RCO_2H^*(\text{2-D, c})/M[Cl^-]/M \quad (1)$$

$$RCO_2H^*(\text{2-D, c})/M[Cl^-]/M \xrightarrow[\text{diffusion}]{\text{surface}} RCO_2H^*(\text{3-D})/M[Cl^-]/M \quad (2)$$

$$RCO_2H(\text{3-D})/M[Cl^-]/M + O_2(g) \rightarrow RCO_2H^*(\text{3-D})/M[\text{oxide}]/M \quad (3)$$

$$RCO_2H^*(\text{3-D})/M[\text{oxide}]/M \xrightarrow[\text{diffusion}]{\text{surface}} RCO_2^-(\text{2-D})/M[\text{oxide}]/M \quad (4)$$

These processes also are summarized graphically in Figure 8. On Ag, Cu, and Al, the native oxide layers exhibit sufficiently basic properties that deprotonation of the adsorbing RCO_2H molecules occurs as part of the self-assembly process with formation of a carboxylate surface species, as indicated by the initial state in Process 1, where (2-D, c) denotes a quasi-two-dimensional, crystalline film.

Upon exposure to HCl, Process 1 converts $-CO_2^-$ to CO_2H, while in parallel, although on a somewhat different and undetermined time scale, the initial native oxides can undergo reaction to form metal chloride layers. These processes require permeation of the HCl molecules into the SAM structure. This permeation appears to occur on a time scale of seconds or less as indicated by the complete rearrangement of the Ag SAMs with only a 10-s HCl exposure. Since these Ag SAMs exhibit a structure as highly organized as on any other substrate studied, e.g., as indicated by our IRS and wetting data, and since the basiscity of the $-CO_2^-$ head groups should be the same for all SAMs, it would appear that the difference between the behavior of comparable chain length SAMs on different substrates is predominantly due to differences in substrate chemistry.

Conversion of the metal oxide to a chloride results in a strong diminution of the substrate basicity, thereby removing the driving force for any deprotonation of the newly formed $-CO_2H$ head groups and leaving the RCO_2H molecules predominantly held to the surface by van der Waals forces of considerably smaller magnitude than the original ionic forces at the $-CO_2^-$/substrate interface. These physisorbed RCO_2H species are indicated by an asterisk to indicate their thermodynamic instability relative to the original SAM structure. Since it was concluded above that HCl permeation and $-CO_2^-$ protonation rates should be similar on all the SAMs, the observation that the SAM/Al system is highly resistant to the effects of HCl implies that Process 1 is inhibited because of the chemical stability of the Al_2O_3 lattice toward HCl attack. This conclusion fits with the observation that formation of $AlCl_3$ is only observed at very high temperatures[38] and suggests that complete protonation of the CO_2H head group arises only when the intrinsic basic property of the substrate is removed by drastic chemical alteration of the adsorbent lattice. In the cases of Ag and Cu irreversible reaction with HCl is expected. For example, the strong adsorption of Cl adatoms on silver surfaces has been reported for both Cl_2[39] and HCl exposure.[40] In the particular case of the evaporated silver films used in the present study, our XPS results confirm that exposure of a freshly vacuum deposited Ag surface to HCl vapor for a few seconds results in formation of a Cl adlayer with an accompanying diminution of the surface O concentration.[41] The importance of the lattice chemistry as the critical driving force for Process 1, relative to a protonation driving force, is shown also by the observation that exposure of H_2S, a quite weak acid but active sulfiding agent, to Ag and Cu SAMs induces protonation and reorganization similar to that observed with HCl on the same types of SAMs.[42]

The kinetically trapped RCO_2H^* state, formed in Process 1 for Ag and Cu, apparently relaxes by formation of microscopic

(38) Kasaoka, S.; Sakata, Y.; Shirata, M. *Nippon Kagaku Kaishi* **1977**, *11*, 1728−1736.

(39) Bowker, M.; Waugh, K. C. *Surf. Sci.* **1983**, *134*, 639−664. Goddard, P. J.; Lambert, R. M. *Surf. Sci.* **1977**, *67*, 180−194. Schott, J. H.; White, H. S. *J. Phys. Chem.* **1994**, *98*, 291−296.

(40) Graedel, T. E. *J. Electrochem. Soc.* **1992**, *139*, 1963−1970. Rice, D. W.; Peterson, P.; Rigby, E. B.; Phipps, P. B. P.; Cappell, R. J.; Tremoureux, R. *J. Electrochem. Soc.* **1981**, *128*, 275−284.

(41) For example, using the standard 10-s exposure time, both clean Ag and Ag/SAM samples were exposed to HCl vapor. Before exposure no peaks were observed in the 180−280 eV Cl2p and 2s core-level region while the standard O1s core-level peak was observed. After exposure, $Cl2p_{3/2}$, 2p1/2, and 2s1/2 peaks were observed at 197.31, 198.92, and 268.36 eV, respectively, while the O1s peak was strongly diminished. Over the course of 3 days ambient exposure in a closed container, the Cl peaks were seen to decrease in intensity by a factor of ∼3 while the O core level peaks begin to reappear indicating reformation of the surface oxide.

(42) Tao, Y. T. Unpublished Results.

domains of 3-D phases with the specific phases dependent upon the specific alkyl chain length and the substrate metal. This is summarized in Process 2 where RCO_2H(3-D) represents some 3-D structure. This quasi-2D → 3-D change is analogous to a wetting−dewetting or roughening transition induced by a sudden shift in the interfacial energy. In the case of the C_n/Ag SAMs, where substantial variations of n were carried out, the IRS data show that for $n < 14$ liquid-like, disordered phases form, indicating that cohesive chain−chain interactions are competing with thermal disordering forces and random substrate pinning which prevent crystal nucleation. For the C11 to C13 acids, the melting points are all above ambient temperature, 28, 44, and 41 °C, respectively, so the thermodynamically favored bulk form is a crystal. However, for $n > 14$, HCl exposure can result in formation of highly ordered crystalline phases which are representative of the stable phases observed in normal bulk crystals of the acids. For example, in the case of the C16 acid, a monoclinic phase forms. This 3-D phase offers a lower energy state than the 2-D RCO_2H* one by providing stabilization via H-bonding in the $[CO_2H]_2$ dimer while further increasing the chain packing interactions to that of a dense ordered crystal. In addition, the IRS data show that for the C16 SAM/Ag the {010} or {100} monoclinic crystal surface planes are oriented near parallel to the substrate surface, an arrangement which keeps the alkyl chains aligned along the surface and thereby maximizes the crystallite/substrate van der Waals interactions.[43] The corresponding reorganization process for crystallite formation, particularly in the final stages, requires substantial molecular diffusion along the surface to the nucleation/growth sites. Our estimated crystallite size of ∼50 Å for the C16 case sets an average intercrystallite spacing of this order (see Figure 8 for a rough graphic indication). Diffusion of RCO_2H molecules over such distances on the time scales of seconds to minutes seems quite reasonable. For the case of the longer chain C24/Ag SAM, the IRS C−H stretching region spectra (compare Figures 3 and 10) indicate a tendency for the HCl exposure to induce similar acid microcrystallite formation as with the C16 SAM, but the low-frequency spectrum in Figure 10 shows that not all $-CO_2^-$ species become protonated in the C24 SAM. These data indicate that the longer chain length makes the SAM more resistant to reorganization, a point which will be discussed below in more detail. Finally, the behavior of the C16 SAM on a Cu substrate is somewhat different than for Ag. The similarity of the IRS C−H stretching spectra of the two post-HCl SAMs (compare Figures 3 and 12) indicates that film de-wetting occurs on Cu with formation of discrete islands of adsorbate species, but the distinctly higher intensity ratio of the $-CO_2^-/CO_2H$ features on Cu indicates that the specific species involved are quite different in the two cases with formation of bulk-like phases of C16 acid crystallites only of minor importance on Cu. This result appears quite consistent with the complex chemisorption chemistry known for Cu surfaces.[35,36,37]

Long-term ambient O_2 exposure of the reorganized HCl-exposed SAMs allows re-oxidation of the substrate metals to form fresh native oxide layers, as indicated in Process 3. In the case of Ag, the adsorbed chloride layer has been shown to be effective in passivating the surface against oxygen adsorption for up to 2 h, after which the oxide layer begins to reform, probably involving migration of the AgCl layer into the bulk.[39] Re-formation of the basic oxide creates a thermodynamically unfavorable state for the acidic CO_2H groups, indicated as the unstable species RCO_2H* in Process 3, and provides a driving force for re-wetting of the substrate and proton transfer, according to Process 4. In agreement with this, air exposure of an HCl-exposed C16/Ag SAM results in formation of the near-identical, original film structure over the course of days, as shown both by the IRS and wetting data. This re-wetting process, as with the original de-wetting step, again requires substantial molecular diffusion along the surface with a significant degree of intrinsic reversibility in order that the highly organized packing, a quasi-equilibrium state, of the original SAM can be achieved. However, complete reversibility is not achieved as shown by a larger contact angle hysteresis on the recovered film surface as compared to the original C16 SAM. This observation implies a greater structural heterogeneity, possibly due to higher defect density within the monolayer and/or roughening of the substrate surface. At the longest chain lengths, kinetic effects appear to be important in determining the course of the reorganizations via Process 4. For example, in strong contrast to the complete return of the HCl-exposed C16 SAM to the original state over 9 days ambient exposure (Figure 3), during the same time span, the C24/Ag SAM continues to restructure as a mixture of RCO_2H and RCO_2^- species, as seen from the spectra in Figure 10. The implication is that for systems with sufficiently large cohesive energies, a total resistance to reorganization may occur.[44] Re-oxidation of the Cu[Cl^-] substrate surface also occurs upon ambient expo-

(43) An important issue which arises with respect to the stability of a crystallite of nanometer-scale dimensions is that of the rapidly increasing free energy with diminishing size as given by the Kelvin relationship: $RT\ln(p/p_0) = 2\gamma V_m/r_c$, where p and p_0 are the vapor pressures of the crystallite and the bulk material, R is the gas constant, T is the temperature, γ is the surface tension, V_m is the molar volume, and r_c is the radius of the crystallite, assumed to be a sphere. Assuming that the surface energy of a long-chain fatty acid crystal is close to that of a long-chain hydrocarbon material sets γ in the neighborhood of 35 ergs/cm^2. Using $V_m \sim 0.27$ L/mol (density of 0.96 g/cm^3) gives values of $p/p_0 \sim 20$, 42, and 1800 for n-hexadecanoic crystallites with diameters of 50, 40, and 20 Å, respectively, at 300 K. This indicates the increasingly strong dissociative instability of isolated (gas phase) nm-size crystallites as the sizes shrink. Evaporative loss under equilibrium conditions can be estimated for n-$C_{15}H_{31}CO_2H$ crystallites using $p_0 \sim 5 \times 10^{-5}$ Torr [extrapolated from data given in: Yaws, C. L. *Handbook of Vapor Pressures*; Gulf Publishing Co.: Houston, TX, 1994; Vol. 3, p 387] which gives corresponding vapor pressures at 300 K of ∼0.0010, 0.0021, and 0.0090 Torr respectively for the diameters above. Given that a typical ∼25 cm^2 SAM film contains ∼1.25×10^{16} molecules (∼5 molecules/nm^2) and that the total gas (ideal) content in the ∼5 cm^3 volume of the sample storage containers at 300 K is ∼1.45×10^{17}, 3.4×10^{15}, and 1.6×10^{15} molecules at the respective vapor pressures above, the percent losses of the crystallites by equilibrium partitioning of the vapor into the container volume would be ∼1, 3, and 100% for the 50, 40, and 20 Å crystallites, respectively, with diameters ≤20 Å leading to significant instability. However, on one hand, these values represent a lower limit of loss since the storage containers were frequently opened and the samples held in the open for extended times during periodic analysis. On the other hand, the stabilities of the crystallites should be higher than indicated since additional stabilization should arise from attractive interactions with the substrate surface. In particular, the long-range van der Waals potential of the substrate will fall off with distance as $\sim z^{-2}$ and thereby impart significant stability to several layers of alkyl chains into the crystallite. Since the experimental observations indicate near total conservation of material on the surface over many days it is clear that the crystallites are, in fact, quite stable. However, since it is not likely that this stability is due to kinetic factors, considering the extremely high surface/volume ratios of the crystallites, the above thermodynamic analysis suggests that the crystallite size distribution actually may be heavily skewed to favor larger sizes, close to the value of ∼5 nm derived from our IRS analysis. Growth of crystallites significantly larger than this size becomes diminishingly unlikely since the intercrystallite spacings will become huge on the molecular scale, a situation which would seem to conflict with the efficient surface diffusion required for the observed formation of C16 acid crystallites over periods of seconds during HCl exposure.

(44) For example, upon introduction of a biphenyl moiety into the alkyl chain, the same HCl exposure results in protonation of the $-CO_2^-$ head group but only minor changes in the IRS spectrum of the C−H stretching region [Tao, Y. T., Unpublished results]. Further evidence for structural reorganization resistance is given by studies of multilayer Langmuir−Blodgett (LB) films of cadmium eicosonate. Relatively long exposure times are reported for protonation of LB films on CaF_2 and Ge by HCl [Saito, M.; Tabe, Y.; Saito, K.; Ikegami, K.; Kuroda, S.; Sugi, M. *Jpn. J. Appl. Phys.* **1990**, *29* (10), 1892−1894] and on Si by HI [Pike, J. K.; Byrd, H.; Morrone, A. A.; Talham, D. R. *J. Am. Chem. Soc.* **1991**, *115*, 8497−8498], and reorganization of the hydrocarbon packing is observed in neither case.

sure. However, the rate may be much faster than for the case of Ag as indicated by the apparent inability of the HCl exposure to induce significant protonation of the C16 CO_2^- species (see Figure 12, low-frequency spectrum). This observation may mean that the chloride adlayer is a poor barrier to oxide formation such that the recovery time for re-establishing the oxide layer after HCl exposure may be comparable to the minimum sample analysis time (<30 min).[45] In addition, the IRS spectra (Figure 12) show that during the course of exposure to O_2 the post-HCl C16/Cu film does not reversibly revert back to the initial organized SAM structure. Rather, the film becomes reorganized into some complex, disorganized form. This may be related to the amorphous nature and/or a restructuring of the oxide layer.

For $n < 14$, the IRS data (Figures 9 and 11) show that the HCl-exposed SAMs on Ag exist initially as disordered RCO_2H phases. However, upon ambient storage they undergo deprotonation (Process 4) to form RCO_2^- phases but these phases remain more disordered than the original SAM. If the re-formed oxide were identical to the original and if the total number of molecules were conserved from the original SAM, then the inability to form the original SAM structure would appear to be due to kinetic constraints. Unfortunately, the present data do not allow quantitative evaluation of these two conditions without additional analyses. The data do show that the ambient-exposure phases are a complex mixture of states which are different from either the HCl-exposed phases or the original SAM. For example, in the case of the C12/Ag SAM, Figure 11 shows broad, liquid-like C−H stretches, an indication of the presence of liquid-like disordered chains, along with well-defined twist/wag progression bands (although at lower intensity than before), an indication of a conformationally ordered chain population. Further, the intense symmetric $-CO_2^-$ stretching absorption with no accompanying CO_2H features shows that the chains are all anchored to the substrate via the $-CO_2^-$ head groups. The possibility that this complexity is the result of surface roughness is not entirely discounted but the near recovery of the original monolayers in the C14−C20 chain lengths serves as evidence to the contrary.

(45) Consistent with this possibility, the growth of a Cu_2O peak at 647 cm^{-1} can be observed in the IRS spectrum over this time scale.

5. Conclusions

In summary, it has been demonstrated that self-assembled monolayers of *n*-alkanoic acids on Ag, Cu, and Al substrates exhibit different time-dependent responses of structural rearrangements upon exposure to HCl vapor. These responses can be understood in terms of a general mechanism involving (1) HCl-induced protonation of the initial $-CO_2^-$ head groups concurrent with a chemical reaction of the basic oxide surface layers to form more neutral chloride layers, (2) rapid stabilization of the formed RCO_2H surface species by structural rearrangements of the quasi-2-D structures to 3-D distributions of domains of bulk-like crystalline and disordered phases, and (3) gradual reversion upon storage in ambient to R CO_2^- monolayer types of films on oxide surfaces formed by re-oxidation of the substrate metal by atmospheric oxygen. While Cu and Ag SAMs undergo all of these processes, although yielding distinctly different types of structures depending upon the alkyl chain length and the substrate metal, Al SAMs are resistant to HCl exposure, apparently because of the chemical inertness of the substrate toward reaction during the exposure period. The most dramatic observation is that HCl exposure of the C16/Ag SAM causes reversible dewetting of the film with formation of surface-adsorbed monoclinic nanocrystals with sizes of 50 ± 7 Å determined by detailed analysis of the IRS spectra.

Acknowledgment. Financial support from the National Science Council, Republic of China, and the National Science Foundation (Grant No. DMR-900-1270) is gratefully acknowledged.

JA960672I